DOI 10.1515/aot-2013-0030 — Adv. Opt. Techn. 2013; 2(4): 337–344

Review Article

Brenden Scott Nickerson and Hans Jürgen Kreuzer*

Deconvolution for digital in-line holographic microscopy

Abstract: To improve the resolution in point source digital in-line holography, we present two deconvolutions, one for the illumination system (coherent or partially coherent light source such as a laser or diode and pinhole) and one for the finite numerical aperture of the hologram. We show that for a system with moderate numerical aperture, optimal resolution of $\lambda/2$ laterally and λ in depth can be achieved.

Keywords: deconvolution; holography; resolution.

OCIS Classification Code: 090.0090.

***Corresponding author: Hans Jürgen Kreuzer,** Department of Physics and Atmospheric Science, Dalhousie University, Halifax, Nova Scotia B3H 3J5, Canada, e-mail: kreuzer@fizz.phys.dal.ca
Brenden Scott Nickerson: Department of Physics and Atmospheric Science, Dalhousie University, Halifax, Nova Scotia B3H 3J5, Canada

1 Introduction

The precision reached in any physical experiment is ultimately limited by the resolution of the instrument used in the measurement. Thus, the experimental data obtained, $I_E(\boldsymbol{r})$, is the result of a convolution of the optimal data, $I(\boldsymbol{r})$, with the instrument function, $f(\boldsymbol{r})$,

$$I_E(\boldsymbol{r})=\int d\boldsymbol{r}'\, f(\boldsymbol{r}-\boldsymbol{r}')I(\boldsymbol{r}'). \tag{1}$$

Under ideal conditions, when the instrument function is known, one extracts the perfect data using the deconvolution theorem of the Fourier transformation

$$\begin{aligned} I(\boldsymbol{r})&=\mathcal{F}^{-1}[\hat{I}_E(\boldsymbol{p})/\hat{f}(\boldsymbol{p})] \\ \mathcal{F}\{I_E(\boldsymbol{r})\}&=\hat{I}_E(\boldsymbol{p})=\int d\boldsymbol{r} I_E(\boldsymbol{r})\exp[-2\pi i\boldsymbol{p}\cdot\boldsymbol{r}] \end{aligned} \tag{2}$$

In spectroscopy, this technique has led to the amazing quality of optical spectra as early as the 19th century and has evolved together with other techniques to advance digital signal processing both for optical and acoustic data.

In this paper, we will show that deconvolution leads to significant improvements of three-dimensional (3D) images obtained in holography, in particular, with the point source digital in-line holographic microscope (PSDIHM) schematically depicted in Figure 1, with the relevant notation illustrated in Figure 2 [1, 2]. We will show that a twofold deconvolution is needed to achieve maximum improvement of the image quality, i.e., its optimal lateral and depth resolution of $\lambda/2$ and λ, respectively, where λ is the wavelength of the laser. But before we proceed with this objective, we want to point out what is not the intention of this paper, namely, to use the deconvolution theorem as a mathematical and numerical trick simply to solve a convolution integral, such as the Kirchhoff-Helmholtz integral, as discussed frequently in the optical literature [3, 4]. Indeed, for the reconstruction of the holograms, we use a much faster and more flexible, patented algorithm as alluded to below [5]. The focus here is on the application of deconvolution methods as they apply to the instrument functions involved.

We recall that in optics, the propagation of a wave field from one plane to another along the optical path is invariably given in terms of a convolution of the wave amplitude and a propagator, or a Green's function. This (exact) mathematical property always arises when the formal solution of a differential equation is given in terms of an integral equation in which the appropriate boundary conditions are accounted for. In quantum mechanics, this is the Lippmann-Schwinger equation equivalent for particle scattering to the Schrödinger equation. In optics, these are the expressions in scalar theory for solutions of the Helmholtz equation for different approximations or boundary conditions associated, in particular, with the names of Fresnel, Kirchhoff, Helmholtz, Rayleigh, and Sommerfeld [3].

The use of deconvolution to account for instrumental limitations as discussed at the beginning of this paper has been suggested repeatedly to improve the reconstructed images in digital holography, see, e.g., [2]. Also, the

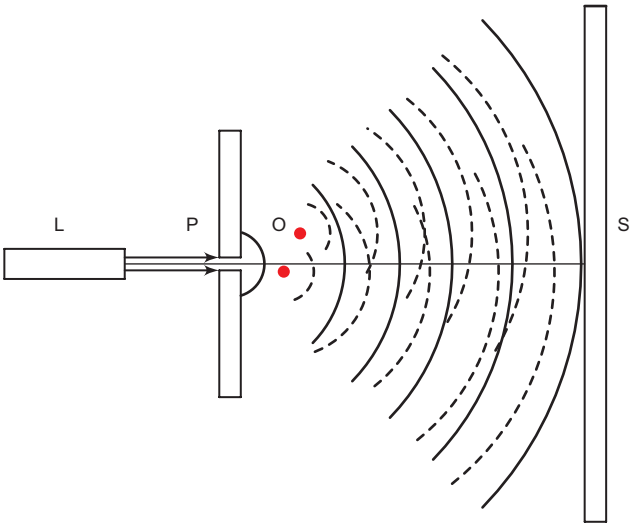

Figure 1 Schematic of DIHM: a coherent or partially coherent light source such as a laser or diode *L* is focused onto a pinhole *P*. The emerging spherical wave illuminates the objects *O*, and the interference pattern or hologram is recorded on the screen *S*. The solid and dashed lines are the reference and scattered wave, respectively.

usefulness of deconvolution in DIHM to improve resolution has been convincingly presented by Latychevskaia et al. [6], although for only 'half' the problem as we will discuss in this paper.

This paper is structured as follows. In the next section, we introduce point source DIHM and formulate the problem of deconvolution. Next, we present results, discuss some numerical issues, and finally draw some conclusions.

2 Point source digital in-line holographic microscopy

In PSDIHM, the light emanating from the point source propagates to the screen with some of it being scattered by the object in front of the source. Thus, the complex wave amplitude at the screen is given by

$$U(\boldsymbol{r})=U_{ref}(\boldsymbol{r})+U_{scat}(\boldsymbol{r}) \tag{3}$$

where $U_{ref}(\boldsymbol{r})$ and $U_{scat}(\boldsymbol{r})$ are the unscattered reference wave and the scattered wave, respectively. The intensity recorded on the screen becomes

$$\begin{aligned} I(\boldsymbol{r}) &= U(\boldsymbol{r})U^{*}(\boldsymbol{r}) \\ &= U_{ref}(\boldsymbol{r})U^{*}_{ref}(\boldsymbol{r})+U_{scat}(\boldsymbol{r})U^{*}_{scat}(\boldsymbol{r}) \\ &\quad +[U_{ref}(\boldsymbol{r})U^{*}_{scat}(\boldsymbol{r})+U_{scat}(\boldsymbol{r})U^{*}_{ref}(\boldsymbol{r})]. \end{aligned} \tag{4}$$

The first term is the intensity of the unscattered part of the reference wave; the second term is the intensity of the scattered wave; it is the subject of classical diffraction theory in wave optics. The two terms in the square brackets represent the interference between the reference and the scattered waves. This is called holographic diffraction and is the basis of holography [1, 2, 7].

Holography is a two-step process: first, a hologram is recorded and stored digitally. Second, a reconstruction is performed to obtain the 3D structure of the object from the 2-D hologram on the screen or, in technical terms, to reconstruct the wave front at the object. In DIHM, this is done numerically based on the theory of wave propagation in optics, i.e., by backward diffraction of the digitally stored pattern on the 2-D hologram via the reference wave. This diffraction process is given in scalar diffraction theory by the Fresnel formula, the Kirchhoff-Fresnel transform, or the Rayleigh-Sommerfeld integral, all of which are approximate solutions to the Helmholtz equation for different boundary conditions. As already discussed by Born and Wolf, these solutions do not differ significantly in the optically important regions, except very close behind a lens. In holographic microscopy, this has also been tested and found that there are no

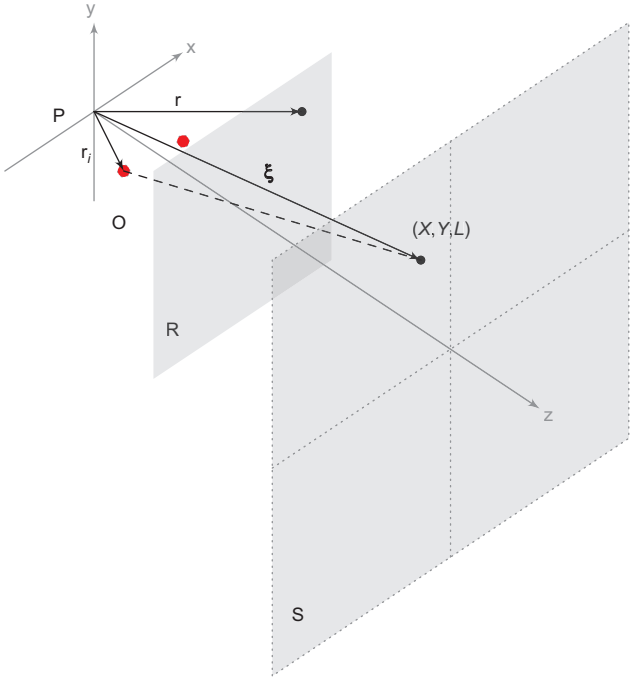

Figure 2 Three-dimensional illustration of the notation for DIHM. Point source *P* located at (0, 0, 0), scatterers *O* located at $\boldsymbol{r}_i=\langle x_i, y_i, z_i\rangle$, reconstruction plane *R* located at $\boldsymbol{r}=\langle x, y, z\rangle$, which is chosen by the user and the recording screen *S* located at $\boldsymbol{\xi}=\langle X, Y, L\rangle$.

significant differences in situations of high magnification, i.e., when the object is placed close to the pinhole. We limit the following discussion to the Kirchhoff-Helmholtz transform

$$K(\boldsymbol{r})=\int_S d\boldsymbol{\xi}\tilde{I}(\boldsymbol{\xi})U_{ref}(\boldsymbol{\xi})\frac{\exp[-ik|\boldsymbol{\xi}-\boldsymbol{r}|]}{|\boldsymbol{\xi}-\boldsymbol{r}|}F_{in}(\boldsymbol{\xi}). \tag{5}$$

Here,

$$\tilde{I}(\boldsymbol{\xi})=I(\boldsymbol{\xi})-U_{ref}(\boldsymbol{\xi})U^{*}_{ref}(\boldsymbol{\xi}) \tag{6}$$

is the contrast intensity, $\boldsymbol{r}$ and $\boldsymbol{\xi}$ are the vectors from the point source to the object and screen, respectively, and $k=2\pi/\lambda$ is the wave number. For a point source, the reference wave is spherical, i.e., $U_{ref}(\boldsymbol{\xi})=\xi^{-1}\exp[-ik\xi]$. Thus, Fresnel's approximation to the inclination factor becomes (for the geometry in which the screen is perpendicular to the optical axis)

$$F_{in}(\boldsymbol{\xi})=-\frac{i}{2\lambda}(1+\cos\chi)=-\frac{i}{2\lambda}\left(1+\frac{L}{\xi}\right) \tag{7}$$

where χ is the angle between the optical axis from the point source to the center of the screen a distance L away, and the vector $\boldsymbol{\xi}$ is in the plane of the screen [2].

Taking the contrast intensity by subtracting the laser intensity at the screen in the absence of the object, one eliminates this dominant term and also, more importantly, any flaws in the laser illumination or camera. This subtraction can be done as just outlined or, if the removal of the object is not practical, one applies a high-pass filter to the hologram [8].

$K(\boldsymbol{r})$ is a complex wave amplitude that can be calculated according to (5) anywhere in space, in particular, in the volume of the object/sample, thus, rendering its 3-D structure if sufficiently transparent. The absolute square $|K(\boldsymbol{r})|^2$ yields the intensity at the object, and its phase gives information about its index of refraction [9]. The numerical evaluation of the diffraction integral is time-consuming even for a 'small' hologram of only $10^3\times10^3$ pixels. Observing that the Kirchhoff-Fresnel integral is a convolution, one is tempted to use fast-Fourier transforms for its deconvolution. To do this, one needs to digitize (5) as the hologram, itself, is of course given in digitized form, $\boldsymbol{\xi}\rightarrow(\nu a, \mu a, L)$, where ν and μ enumerate the pixels on the CCD chip, and a is the pixel size. Likewise, one needs to digitize the space coordinates $\boldsymbol{r}\rightarrow(nb, mb, z)$, where b is the size of one pixel in the reconstructed image. Unfortunately, to keep the digitized form of (5), a convolution one needs to make the identification $b=a$, thus, eliminating the opportunity to obtain a magnified image of the object or to use point source DIHM as a viable microscopic technique. To overcome this impasse, several strategies have been explored, most recently, the methods by Kanka et al. [10]. An older, faster, and more efficient procedure is to simplify the diffraction integral, itself [8]. We observe that in DIHM, the distance from the pinhole to the object is typically much smaller than to the screen. Thus, we can use an expansion

$$\begin{aligned}|\boldsymbol{\xi}-\boldsymbol{r}|&\approx\xi\left[1-\frac{2\boldsymbol{\xi}\cdot\boldsymbol{r}}{\xi^2}\right]^{1/2}\\&\approx\xi\left[1-\frac{\boldsymbol{\xi}\cdot\boldsymbol{r}}{\xi^2}-\frac{1}{2}\left(\frac{\boldsymbol{\xi}\cdot\boldsymbol{r}}{\xi^2}\right)^2-\dots\right].\end{aligned} \tag{8}$$

Keeping only the linear term yields the Kirchhoff-Helmholtz transform [8]

$$K(\boldsymbol{r})=-\frac{i}{2\lambda}\int_S d\boldsymbol{\xi}\tilde{I}(\boldsymbol{\xi})\frac{(1+\xi/L)}{\xi^2}\exp[-ik\boldsymbol{\xi}\cdot\boldsymbol{r}/\xi]. \tag{9}$$

Again, the function $K(\boldsymbol{r})$ is complex and significantly structured and different from zero only in the space region occupied by the object. An algorithm has been developed for its evaluation that is outlined elsewhere, faster by many orders of magnitude than the direct evaluation of the double integral [2, 5]. Noteworthy is the fact that in this algorithm, the pixel size in the reconstructed image can be chosen arbitrarily to achieve any magnification one wishes. For high-resolution imaging, i.e., when the object is very close to the pinhole within less than a millimeter, the other methods give very similar results but are not as fast.

Calculating the complex amplitude throughout the object, the local phase and intensity can be obtained

$$\phi(\boldsymbol{r})=\arg(K(\boldsymbol{r})) \tag{10}$$

$$I_{recon}(\boldsymbol{r})=K(\boldsymbol{r})K^{*}(\boldsymbol{r}). \tag{11}$$

In PSDIHM, there are two instrumental features that limit resolution and image quality. Associated with the hologram, itself, is the fact that pinholes are not perfect point sources but have a finite size on the order of the wavelength. The corresponding instrument function is the reference wave with which the hologram should be deconvoluted. Associated with the reconstruction is the limitation of the numerical aperture given by the finite size of the recording chip and its distance from the pinhole. We will address both issues in this paper.

3 Deconvolution for light source and pinhole

As mentioned above, an approximate way to account for the finite pinhole size is to use the contrast hologram obtained by subtracting the background hologram, taken in the absence of the object. This also has the advantage that it removes possible contamination due to laser imperfections and due to the object holder, i.e., a glass slide or small tank. It already leads to a significant improvement in reconstruction as shown in numerous publications [1, 2, 7]. A mathematically more rigorous way is to treat the background hologram as the instrument function and use the deconvolution (2).

If the instrument function, i.e., the background hologram cannot be measured, one can resort to using Airy's function, f_A, or its Gaussian approximation, of a circular aperture as the instrument function in the deconvolution

$$f_A(\boldsymbol{r})=f_0\left[\frac{2J_1(x)}{x}\right]^2 \tag{12}$$

$$x=ka\sin\theta=ka\frac{R}{L} \tag{13}$$

where a is the radius of the pinhole, and R is the radial distance from the optical axis on a screen at distance L. Its numerical aperture, defined via the half angle under which the first zero in Airy's function appears is

$$NA\approx 1.22\,\lambda/(2a)$$

In Figure 3, we show (A) the hologram of 1 µm spheres on a glass slide, (B) the Airy function of a pinhole with diameter 1 µm, (C) the deconvoluted hologram, and (D) the reconstruction, where the red outline refers to the corresponding section seen in Figures 6 and 7.

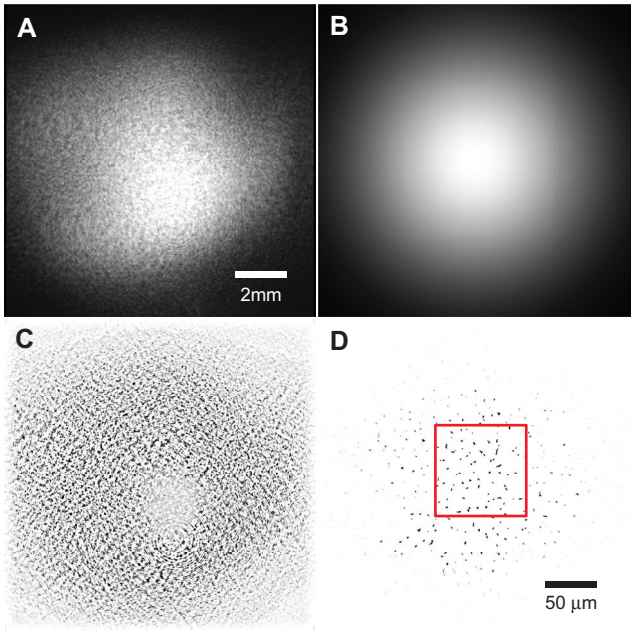

Figure 3 (A) the hologram of 1 µm spheres on a glass slide, (B) the Airy function of a pinhole with diameter 1 µm, (C) the deconvoluted hologram, and (D) the reconstruction, where the red outline refers to the corresponding section seen in Figures 6 and 7.

4 Deconvolution for detector size

The numerical aperture due to the finite screen size is

$$NA=n\sin\alpha$$

where n is the refractive index of the medium between the pinhole and the detector, and α is the half angle under which the detector is seen, i.e., $\tan(D/2L)$, where L is the distance from the pinhole to the center of the screen, and D is its lateral dimension.

To obtain the corresponding instrument or point spread function, f_{NA}, we assume a perfect point source emitting a spherical wave $U_{ref}(\boldsymbol{r})=A_r\exp[ikr]/r$ with wavenumber $k=2\pi/\lambda$. In addition, we have a point object at a distance $\boldsymbol{r}_0$ from which scattered spherical waves emerge. The total wave field is, thus,

$$U(\boldsymbol{r})=A_r\frac{\exp[ikr]}{r}+A_0\frac{\exp[ik|\boldsymbol{r}\text{-}\boldsymbol{r}_0|]}{|\boldsymbol{r}\text{-}\boldsymbol{r}_0|} \tag{14}$$

and the intensity of the contrast hologram becomes

$$\begin{aligned}\tilde{I}(\boldsymbol{r})&=I(\boldsymbol{r})\text{-}\frac{A_r^2}{r^2}\\&=\frac{A_0^2}{|\boldsymbol{r}\text{-}\boldsymbol{r}_0|^2}+2\frac{A_0A_r}{r|\boldsymbol{r}\text{-}\boldsymbol{r}_0|}\cos[k(r\text{-}|\boldsymbol{r}\text{-}\boldsymbol{r}_0|)]\end{aligned} \tag{15}$$

The first term accounts for classical scattering from an isolated object resulting in a smoothly varying background. The second term is due to interference between the source and the object and represent holographic interference. Under holographic conditions, we must have $A_r>>A_0$. With the contrast hologram given on a screen with numerical aperture NA, we can use the Kirchhoff-Helmholtz transform to calculate the reconstructed intensity around the original point source at $\boldsymbol{r}_0$. This point

spread function has been obtained analytically [8] and is given exactly by

$$f_{NA}(\boldsymbol{r})=|k_{NA}(\boldsymbol{r})|^2 \tag{16}$$

$$k_{NA}(\boldsymbol{r})=2\sum_{n=0}^{\infty}a_n i^n P_n\left(\frac{z}{|\boldsymbol{r}|}\right)j_n(k|\boldsymbol{r}|) \tag{17}$$

$$a_n=(n+1/2)\int_{\sqrt{1-(NA)^2}}^{1}dtP_n(t) \tag{18}$$

It is easily evaluated numerically but can also be approximated by products of Gaussians

$$f_{NA}(x)\approx\frac{1}{\sqrt{\pi}}\exp[-x^2/\delta^2]$$

with the widths given by Rayleigh's criterion

$$\delta=\delta_{lat}\approx\frac{\lambda}{2NA}$$
$$\delta=\delta_{long}\approx\frac{\lambda}{(NA)^2}$$

for lateral and longitudinal resolution, respectively. The point spread function is shown in Figure 4 in two sections, perpendicular and parallel to the optical axis. Thus, the 3-D reconstruction of a hologram generated for a point scatterer somewhere between the pinhole and the screen will be seen as an ellipsoidal 'football' with its long axis along the optical axis. To clarify the deconvolution for the detector size, let us assume the object is given by a 3-D pixel array of δ-functions. Using PSDIHM, we obtain an image for a numerical aperture NA that is given by a set of such 'footballs', i.e.,

$$I_{NA}(\boldsymbol{r})=\int d\boldsymbol{r}'\, f_{NA}(\boldsymbol{r}-\boldsymbol{r}')I(\boldsymbol{r}'). \tag{19}$$

Deconvolution will then produce the optimal image $I(\boldsymbol{r})=I_{NA=1}(\boldsymbol{r})$, which is now an array of minimal 'footballs' with the long and short axes of lengths λ and $\lambda/2$, respectively, as the maximal resolution in our instrument, i.e., we cannot, in principle, recover the δ-functions, not even with an infinitely large detector.

The deconvolution can be done at two levels, namely, with the reconstructed intensity $I_{NA}(\boldsymbol{r})$ or with the reconstructed amplitude $K_{NA}(\boldsymbol{r})$. The intensity deconvolution follows the procedure outlined above, given in (2). More care must be given to the amplitude deconvolution.

4.1 Amplitude deconvolution

Amplitude deconvolution is essential if one wants to construct a detailed phase map of the object. Starting from the amplitude (9), we write

$$K_{NA}(\boldsymbol{r})=\int d\boldsymbol{r}'\, k_{NA}(\boldsymbol{r}-\boldsymbol{r}')K(\boldsymbol{r}'). \tag{20}$$

and get

$$\begin{aligned}K(\boldsymbol{r})&=\mathcal{F}^{-1}\left[\hat{K}_{NA}(\boldsymbol{p})/\hat{k}_{NA}(\boldsymbol{p})\right]\\&=\mathcal{F}^{-1}\left[\hat{K}_{NA}(\boldsymbol{p})\hat{k}^{*}_{NA}(\boldsymbol{p})/\widehat{psf}_{NA}(\boldsymbol{p})\right]\end{aligned} \tag{21}$$

from which we can calculate both the intensity and the amplitude. A practical difficulty with amplitude deconvolution is phase wrapping, i.e., the fact that the phase

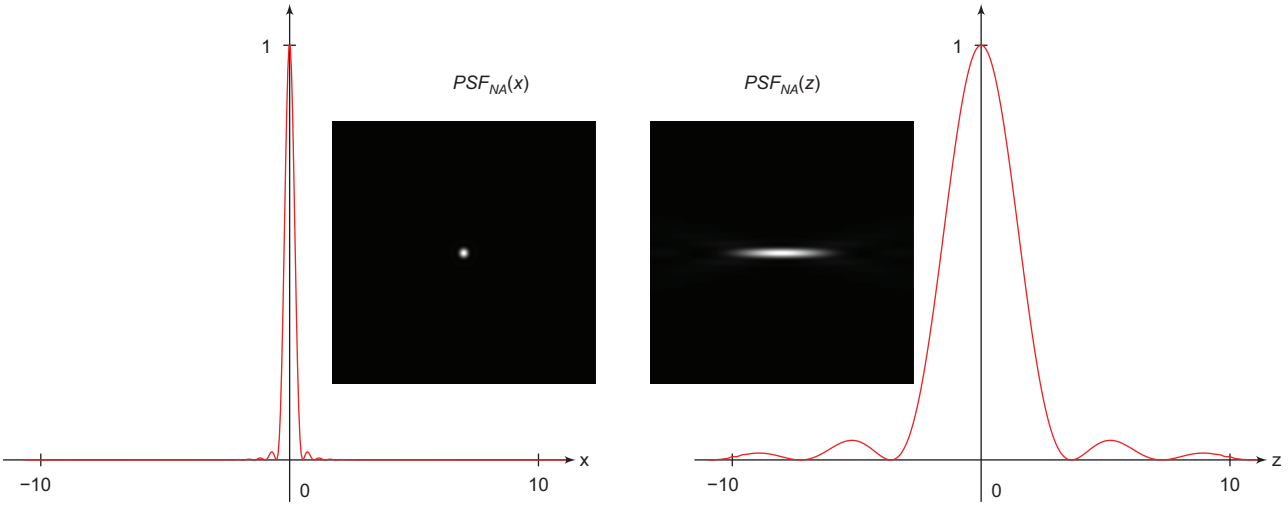

Figure 4 Point spread function, given by (16), in the planes perpendicular (x,y) and along the optical axis (x,z).

of $K(\boldsymbol{r})$ is only given modulo π. This is a serious numerical problem when a 3-D stack of amplitude maps on planes perpendicular to the optical axis is assembled as the phase must be followed from one plane to the next. If that is not done properly, depth resolution is severely affected or even lost. It has been resolved with considerable success in a 2-D phase map from which changes in the index of refraction of the core of an optical fiber has been measured with PSDIHM to four digits [9].

4.2 Noise

The numerical implementation of the deconvolution via FFTs runs into difficulties because any measured image has noise in it, assumed here to be white noise

$$\tilde{I}_{NA}(\boldsymbol{r}) = I_{NA} + I_{noise}.$$

Its Fourier transform is

$$\hat{\tilde{I}}_{NA} = \hat{I}_{NA} + \hat{I}_{noise} \tag{22}$$

$$\hat{I}_{noise} = I_0. \tag{23}$$

Once deconvolved using (2), the latter contributes a term

$$I_{noise}(\boldsymbol{r}) \approx \mathcal{F}^{-1}[\, I_0 \exp[\, p^2\delta^2\,]\,]$$

in the inverse transform for a Gaussian point spread function. The largest argument in the exponential is $4\pi^2N^2$, i.e., numbers by far too large for numerical computations except for very small and unreasonable N. This difficulty does not arise for the first term $\hat{I}_{NA}$ as it decreases at about the same rate as the point spread function.

To circumvent this noise difficulty, several methods exist; foremost is the Wiener filter in which one adds or subtracts a constant from the noise term, which is changed iteratively until numerical overflows disappear, and the inverse Fourier transform is stable [6].

4.3 Exact deconvolution or iterative methods

To avoid or remove noise in signal processing of optical or acoustic wave fields or images, iterative methods have been developed, in particular, the Richardson-Lucy algorithm. One must be aware that such methods do not always converge. One can impose arbitrary criteria that stop the iteration when a certain noise reduction has been achieved, and the quality of the signal is judged to be acceptable. However, such criteria are impossible to formulate if the details of the object to be revealed are not known. As an example, in the recording of a voice, one is successful when enough words can be identified. However,

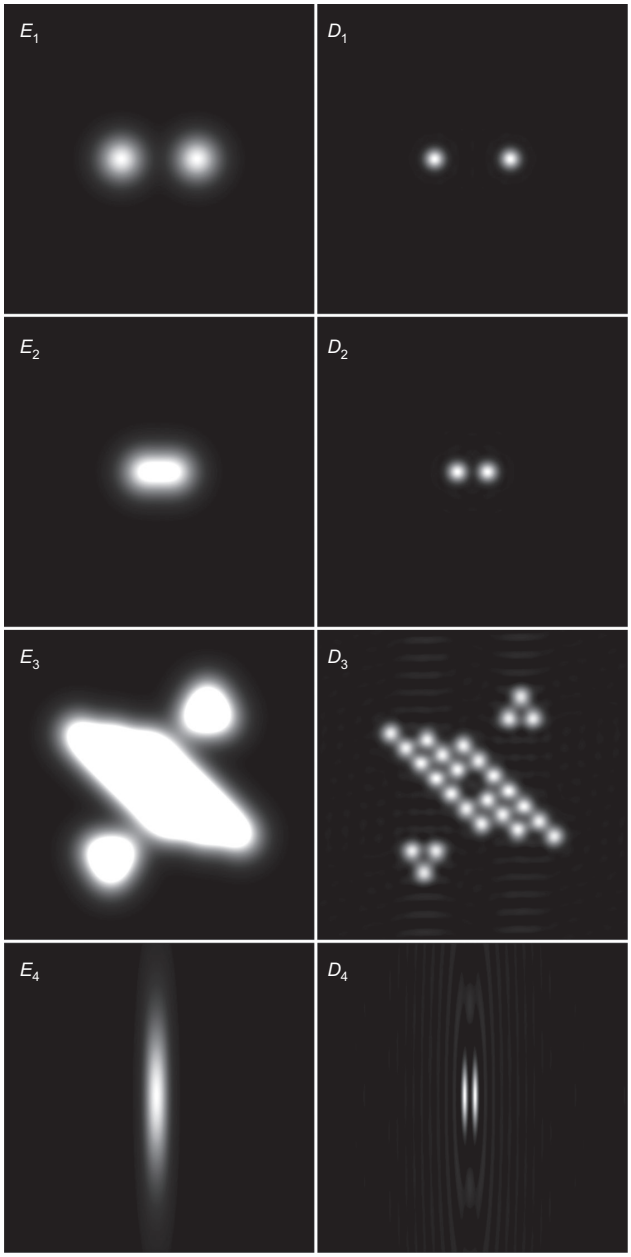

Figure 5 Deconvolution of Gaussian sources. $E_{1,2,3,4}$ are the simulated images with two sources clearly resolved, two sources unresolved, and multiple sources, respectively. $D_{1,2,3,4}$ are the corresponding deconvolutions. E_4, D_4 are along the optical axis as examples of the improvement of depth resolution. NA=0.25 for λ=600 nm.

for the 3-D structure of an unknown algae recorded with DIHM, such criteria are impossible. Proceeding with enough iterations, one eventually arrives at a picture where only the highest intensity pixels survive, i.e., as an example, an image of beads will result in an array of point sources of arbitrarily small radii. On the other hand, this arbitrariness is not present if the deconvolution issues the appropriate instrument functions. Latychevskaia et al. [6] have achieved considerable success in this direction.

5 Some examples

We begin with the simple case of two points being well separated in a plane perpendicular to the optical axis showing images before and after deconvolution (Figure 5). The half-width of the points after deconvolution is $\lambda/2$ as expected for maximum resolution.

Next, we show a similar geometry but with the two points so close that at a numerical aperture NA=0.25, they cannot be resolved anymore. Deconvolution solves this problem (see Figure 5). Last, we look at a clusters of point sources, which at NA=0.25 show up in reconstruction as white blobs, which deconvolution resolves into individual structures.

In an earlier paper on immersion holography [11], we used clusters of 1 μm beads that were poorly resolved in air but clearly resolved in oil. We have taken both images and deconvoluted them with the respective numerical aperture resulting in a further improvement of resolution (see Figures 6 and 7).

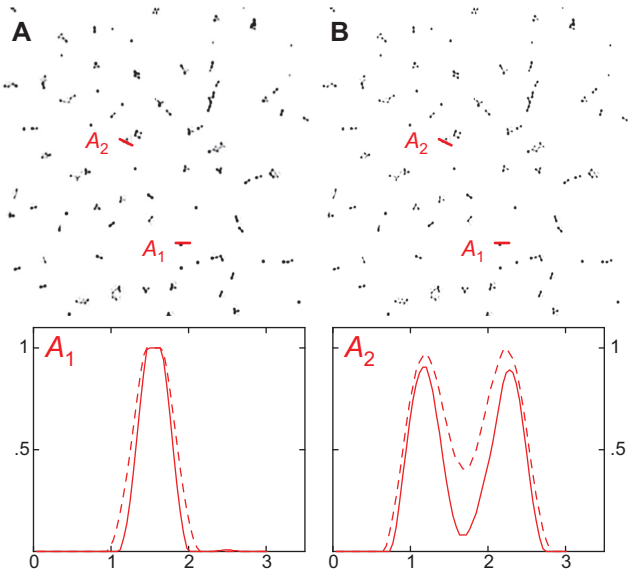

Figure 7 (A) One-micrometer spheres on a glass slide in oil before deconvolution (dashed cuts) and (B) after deconvolution (solid cuts). The cuts are indicated in the upper picture. NA=0:55.

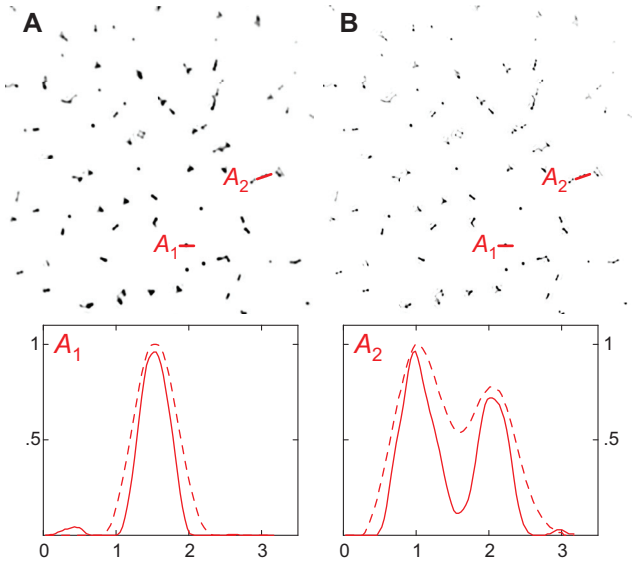

Figure 6 (A) Corresponding to Figure 3 (D), 1-μm spheres on a glass slide in air before deconvolution (dashed cuts) and (B) after deconvolution (solid cuts). The cuts are indicated in the upper picture. NA=0:39.

6 Final comments

Holography is a two-step process consisting of, first, taking a hologram and, second, reconstructing the wavefront at the object creating an image thereof. As a result, there are two instrument functions and consequent convolutions to be considered: first, for the illumination system (laser and pinhole) and, second, for the finite numerical aperture of the recording screen. Both issues have been addressed and resolved in this paper for PSDIHM so that optimal lateral and depth resolutions of $\lambda/2$ and λ, respectively, can be obtained after images are deconvolved. One should note, however, in some situations, not enough of the initial diffraction pattern is recorded by the screen to yield optimal resolution upon deconvolution. This is, of course, a function of the parameters of the microscope, namely, the numerical aperture and wavelength used in the experiment.

A final cautionary note on depth resolution. If optically dense, nontransparent regions in the object are larger than a few wavelengths the impinging waves cannot diffract

sufficiently around the edges and behind the object. In this shadow region, no details can be revealed, not even with holography. The obvious way out of this dilemma is holographic tomography [12] with several point sources impinging on the object from different directions. A very elegant way to do this is the array illumination developed in Jena [13, 14].

Received May 31, 2013; accepted June 24, 2013

References

[1] J. Garcia-Sucerquia, W. Xu, S.K. Jericho, P. Klages, M.H. Jericho, et al., Appl. Opt. 45(5), 836–850 (2006).
[2] M.H. Jericho and H.J. Kreuzer, in 'Coherent Light Microscopy, Chapter 1 Point Source Digital In-Line Holographic Microscopy', (Springer, NY, 2011), pp. 3–30.
[3] M. Born and E. Wolf, in 'Principles of Optics', 7th edition (Cambridge University Press, NY, 1999).
[4] J.W. Goodman, in 'Introduction to Fourier Optics', 2nd edition (McGraw Hill, NY, 1996).
[5] H.J. Kreuzer, US. Patent 6411406 B1, Canadian Patent CA 2376395 (2002).
[6] T. Latychevskaia, F. Gehri and H.W. Fink, Opt. Express 18(21), 22527–22544 (2010).
[7] W. Xu, M.H. Jericho, I.A. Meinertzhagen and H.J. Kreuzer, Appl. Opt. 41(25), 5367–5375 (2002).
[8] H.J. Kreuzer, K. Nakamura, A. Wierzbicki, H.W. Fink and H. Schmid, Ultramicroscopy 45(3–4), 381–403 (1992).
[9] M.H. Jericho, H.J. Kreuzer, M. Kanka and R. Riesenberg, Appl. Opt. 51(10), 1503–1515 (2012).
[10] M. Kanka, R. Riesenberg and H.J. Kreuzer, Reconstruction of high-resolution holographic microscopic images. Opt. Lett. 34(8), 1162–1164 (2009).
[11] J. Garcia-Sucerquia, W. Xu, M.H. Jericho and H.J. Kreuzer. Immersion digital in-line holographic microscopy. Opt. Lett. 31(9), 1211–1213 (2006).
[12] S.K. Jericho, M.H. Jericho and H.J. Kreuzer, in 'Holography – Culture, Art, and Information Technology', Ed. By T.H. Jeong (Scientific and Technical Documentation Press, Beijing, 2010). Proceedings of 8th International Symposium of Display Holography, Shenzhen, China July 12–17, 2009.
[13] P. Petruck, R. Riesenberg, U. Hübner and R. Kowarschik, Opt. Commun. 285(4), 389–392 (2011).
[14] C. Graulig, M. Kanka and R. Riesenberg, Opt. Express 20(20), 22383–22390 (2012).

Brenden Scott Nickerson, BSc Hon. Physics 2014 (Dalhousie). Research in holography since 2011 under the supervision of H. J. Kreuzer.

Hans Jürgen Kreuzer, MSc 1966 (Bonn), Dr. rer. nat. 1967 (Bonn), Professor of Physics U. Of Alberta 1971–1982, Killam Research Professor and A.C. Fales Professor of Theoretical Physics, Dalhousie University since 1982. Publications: 300 papers, 6 books, 260 invited talks, 5 patents. Worked in elementary particle theory, condensed matter, non-equilibrium statistical mechanics, surface science, polymer science, holography, physics and chemistry in high electric fields. Honors and Awards: Lady Davies Professor, Technion, Haifa, Israel (1977), Guest Fellow of the Royal Society, London (1987), Fellow of the Max-Planck Society, Germany (1988), Heinrich-Welcker Guest Professor, University of Erlangen-Nuremberg, Germany, 1992, Fellow of the Royal Society of Canada (1993), Humboldt Research Prize (1995, 2008), Guest Professor, Wuhan Institute of Technology, China.